Structural Engineering and Mechanics, Vol. 42, No. 2 (2012) 131-152

DOI: http://dx.doi.org/10.12989/sem.2012.42.2.131

Effects of geometric parameters on in-plane vibrations of two-stepped circular beams

Ekrem Tufekci* and Oznur Ozdemirci Yigit[a]

Faculty of Mechanical Engineering, Istanbul Technical University, Gumussuyu, TR34437 Istanbul, Turkey

(Received July 9, 2011, Revised February 7, 2012, Accepted March 7, 2012)

Abstract. In-plane free vibrations of circular beams with stepped cross-sections are investigated by using the exact analytical solution. The axial extension, transverse shear deformation and rotatory inertia effects are taken into account. The stepped arch is divided into a number of arches with constant cross-sections. The exact solution of the governing equations is obtained by the initial value method. Several examples of arches with different step ratios, different locations of the steps, boundary conditions, opening angles and slenderness ratios for the first few modes are presented to illustrate the validity and accuracy of the method. The effects of the geometric parameters on the natural frequencies are investigated in details. Several examples in the literature are solved and the results are given in tables. The agreement of the results is good for all examples considered. The mode transition phenomenon is also observed for the stepped arches. Some examples are solved also numerically by using the commercial finite element program ANSYS.

Keywords: curved beam; stepped arch; free vibration; in-plane; exact solution; mode transition

1. Introduction

Engineering structures often consist of a number of components that can be modelled as beams, curved beams and rings. Curved beams are one of the most predominant components in engineering structures. Curved structural members are widely seen our surroundings, such as railway supports in a playgrounds resembling a C-ring structure, vehicle chassis and frame structures. It has been recorded that the free vibration of curved beams has been the subject of much work due to their many practical applications. More than 600 articles have been summarized in review articles (Markus and Nanasi 1981, Laura and Maurizi 1987, Chidamparam and Leissa 1993, Auciello and De Rosa 1994). The first studies on this argument date back to the end of 19th century and frequently still appeared in the scientific literature. Considerable amount of attention has been devoted to the analysis of such elements in recent years. The arch bridges are widely used structures in civil engineering and theoretical analysis and experiments are still conducted (Lu *et al*. 2010, Ren *et al*. 2010). The magnet positioner with the C-arm which is intended to be part of a clinical setup whose other major mechanical components include a fluoroscopy system and a motorized patient

*Corresponding author, Professor, E-mail: tufekcie@itu.edu.tr
[a]E-mail: oznur.yigit@siemens.com

table. In medical imaging systems as well as many other branches of engineering, similar structures consisting of straight and curved beam components are common (Tunay *et al*. 2009). Most of cardiovascular stents has the curved section with uniform cross-section. But some of stents has varying cross-section (Jang *et al*. 2010).

The gravity-type fish cage is extensively applied with the increasing demand for fishery products. The flotation ring of a gravity-type fish cage is the main load-bearing component providing the necessary strength of the entire cage in water and supports the whole cage. So it is essential to study the hydro elasticity of the flotation ring for the safety of a fish cage (Dong *et al*. 2010a, b).

Micro-devices such as micro-actuators, micro-switches, micro-mirrors and micro-resonators are widely used in micro-electro-mechanical systems (MEMS) and movable electrode can be modeled as a micro-beam (Hu *et al*. 2010). Micromachined shallow arches have been under increasing focus in recent years in the MEMS community because of their unique attractive features (Younis *et al*. 2010). Vibrations of spiral beams are studied recently as a prelude to sensing and energy harvesting using the piezoelectric effect in MEMS devices. Vibrational energy harvesters convert vibrations available in the environment to electrical energy. The energy generated can be used to power sensor nodes (Karami *et al*. 2010, Zhou *et al*. 2010).

Since their identification in 1991, carbon nanotubes have drawn much attention. A large number of theoretical and experimental studies have been directed toward understanding the static and dynamical behaviors of curved carbon nanotubes due to their enormous applications (Xia and Wang 2010, Ouakad and Younis 2011).

Lin (2008) determined the exact solutions of natural frequencies and mode shapes of a multi-step beam carrying a number of various concentrated mass elements. Then, the same author (Lin 2010) investigated a multi-step beam carrying multiple rigid bars supported elastically.

It must be noted that curved beams are more efficient in the transfer of loads than the straight beams because the transfer is affected by bending, shear and membrane action. The study of the free in-plane vibration of a curved beam using the beam theory is more complex than the analogous problem in a straight beam, since the structural deformations in a curved beam depends not only on the rotation and radial displacements but also on the coupled tangential displacement caused by the curvature of the structure. Many theories have been evolved to derive, simplify and solve the equations of motion for the free in-plane vibration of the curved beams. Generally speaking, all researches relative to this topic can be classified to two categories. One is based on three dimensional elasticity theory, which and the final governing equations involve three or two at least spatial coordinates. The second approach is to transform a three-dimensional elasticity problem to a one-dimensional elasticity problem based on crucial and reasonable hypotheses and neglecting some secondary factors. In this field, the Euler-Bernoulli and Timoshenko theories of beams are two widely used models. The former theory completely neglects shear deformation of the cross-section of beams, while the latter needs to introduce a shear correction factor, which cannot be determined by the theory itself, although shear deformation has been taken into account in this theory.

The curved beam finite elements are the most common tool to analyze the curved beam problems. They are conventionally formulated based upon the displacement fields. Such formulation often leads to excessively stiff behavior in the thin beams. In such analyses, the shear-locking phenomenon occurs when lower order elements are used in modeling. This is because in such models, only flexural deformations are considered and shear deformations are neglected. Another phenomenon is called membrane-locking. It occurs when other classical curved finite elements are used for modeling thin curved beams, because they exhibit excessive membrane stiffness as compared with the bending stiffness in approximating the extensional bending response, and also the lower order element cannot bend without being stretched. It means that such elements are unable to represent the condition of zero radial shear strains. Therefore, these two phenomena are associated with highly undesirable situations and numerical deficiencies. Thus, much attention has been focused on rectifying the locking phenomena.

The common geometry of the curved member consists of a segment of a circular ring with uniform cross-section. However, some curved beams have continuously or discontinuously varying cross-sections. Vibrations of stepped curved beams have been the subject of many papers. The authors examined the vibrations of stepped curved beams with different boundary conditions by using several methods. Verniere De Irassar and Laura (1987) investigated the first symmetric mode of vibration of circular arches. The fundamental frequency coefficients are determined for arches of discontinuously varying cross-sections carrying concentrated masses by means of Rayleigh-Ritz method. Laura *et al.* (1988) presented free vibrations of curved beams having non-uniform thickness by means of the Rayleigh-Ritz method. Two different kinds of stepped curved beams examined for three types of boundary conditions. The effect of concentrated mass was also considered. Gutierrez *et al.* (1989) used polynomial functions and Ritz method to solve in-plane vibrations of curved beams of non-uniform cross-sections. Two types of cross-sectional variations for both symmetrical and unsymmetrical structures were considered, continuous and discontinuous variations for circular and non-circular beams such as parabola, centenary, spiral and cycloid. Balasubramanian and Prathaph (1989) developed a curved beam element for static and dynamic analysis of stepped circular beams by considering the axial extension and shear deformation effects. Rossi *et al*. (1989) studied in-plane vibrations of cantilevered non-circular curved beams of non-uniform cross-sections taking into account a concentrated mass at the free end. The polynomial co-ordinate function was used to calculate the fundamental mode. Ritz method with Rayleigh's optimization criteria was applied to solve the governing equations and finite element method was used to compare the results. Rossi and Laura (1995) introduced the dynamic stiffening effect of hinged and clamped curved beams with discontinuous variations of the cross-sections that was measured by means of the dynamic stiffness efficiency parameter. Tong *et al*. (1998) investigated in-plane free and forced vibrations of circular arches with variable cross-sections under the Kirchhoff's assumptions that take the neutral axis inextensible and neglect the shear deformation and rotatory inertia effects. The circular curved beams having both one step and two steps and also curved beams with continuously varying cross-sections were examined. Liu and Wu (2001) applied the generalized differential quadrature rule based on Kirchhoff assumptions to solve in-plane free vibrations of circular curved beams. Karami and Malekzadeh (2004) applied the differential quadrature method to solve free vibrations of circular curved beams with variable cross-sections by taking into account the effects of axial extension and rotatory inertia. Viola *et al*. (2007) investigated the in-plane linear dynamic behavior of multi-stepped and multi-damaged circular arches under different boundary conditions. Analytical and numerical solutions in undamaged as well as in damaged configurations were obtained. Euler characteristic exponent procedure for analytical solution and generalized differential quadrature element technique for the numerical method were used.

Several examples of arches with uniform, continuously varying and stepped cross-sections are presented by means of a number of approaches such as Ritz, Galerkin, cell discretization, differential quadrature and finite element methods by most of the researchers. Different boundary conditions are examined and comparison of results of different solution methods is performed by neglecting the axial extension, transverse shear deformation and rotatory inertia effects. It can be

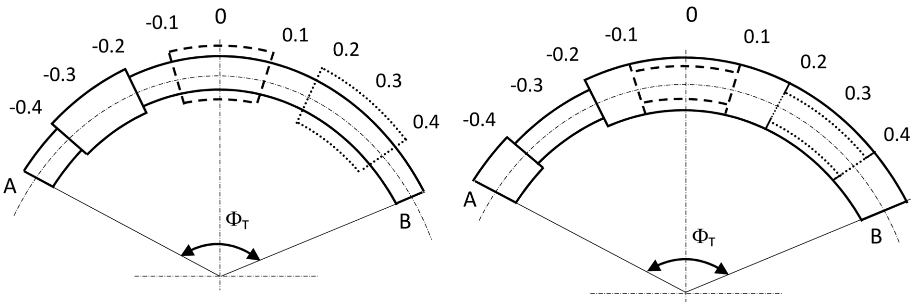

Fig. 1 The different positions of step for $\eta = h_2/h_1 > 1$ and $\eta = h_2/h_1 < 1$

possible to obtain reasonable results for a thin and deep arch by neglecting axial extension effect as well as shear deformation and rotatory inertia effects, even in higher modes. But for a thick and shallow arch, all the effects have to be taken into account for obtaining acceptable results, even in lower modes. For the free vibration of a shallow arch, the axial extension effect is the most important effect among them. A phenomenon of transformation of modes from extensional into inextensional, which occurs with increase in beam curvature, has been observed by several authors (Tarnopolskaya *et al.* 1996, Tarnopolskaya *et al.* 1999, Tufekci 2001). The transformation phenomenon is characterized by the sharp increase in frequencies of modes that occurs at certain combinations of curvature and length of the beam. This increase in mode frequencies is accompanied by a significant change in the mode shapes. There is still no comprehensive analysis of the transformation phenomenon and there are no proper explanations and methods for prediction the frequencies of an arch. This is possibly due to the fact that numerical simulations, commonly employed for the analyses, provide little analytical insight into the vibrational problem.

This study focuses on the free vibrations of two-stepped curved beams. The aim of this study is to extend the analysis given by Tufekci and Ozdemirci (2006) for a two-stepped circular beam (Fig. 1). The effects of geometric parameters on the free vibration of a two-stepped circular beam are investigated in details.

The stepped circular beam is divided into a number of arches with constant cross-sections. The governing differential equations are solved exactly for each portion. The differential equations of motion have been solved exactly by Tufekci and Arpaci (1998), taking into account the effects of shear, rotatory inertia and extensibility of the arch axis. The overall solution of the governing equations of free vibration of the stepped arch can be obtained by satisfying boundary conditions at the ends and kinetic and kinematic continuity conditions at the boundaries of each curved portions. The effects of boundary conditions, opening angles, slenderness ratios, position of the stepped portion, step ratios and the opening angle ratios on the natural frequencies for several modes are given in diagrams. The analysis of the mode transition phenomenon in vibrational behavior of a stepped beam is presented.

2. Analysis

The governing equations of free in-plane vibrations of a circular arch with constant cross-section are given by Tufekci and Arpaci (1998).

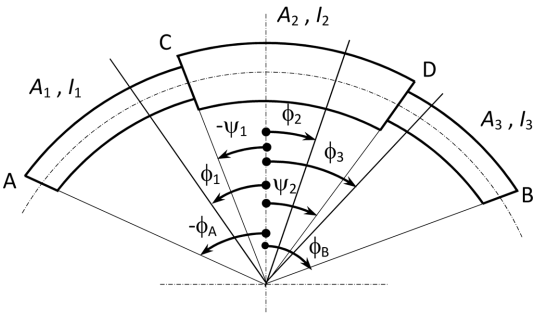

Fig. 2 Geometry of the stepped arch

$$\frac{dw}{d\phi} = u + \frac{R}{EA}F_t \qquad \frac{du}{d\phi} = -w + \frac{RF_n}{GA/k_n} + R\Omega_b$$
$$\frac{d\Omega_b}{d\phi} = \frac{R}{EI_b}M_b \qquad \frac{dM_b}{d\phi} = -RF_n - R\mu\frac{I_b}{A}\omega^2\Omega_b$$
$$\frac{dF_t}{d\phi} = F_n - R\mu\omega^2 w \qquad \frac{dF_n}{d\phi} = -F_t - R\mu\omega^2\Omega \tag{1}$$

where u, w are normal and tangential displacements; Ω_b is the rotation angle about the binormal axis; ϕ is the angular co-ordinate; R is the radius of curvature of undeformed beam axis; F_n, F_t are normal and tangential components of internal force; M_b is the internal moment about the binormal axis; E, G are Young's and shearing moduli; A is the cross-sectional area; I_b is the moment of inertia about the binormal axis; μ is the mass per unit length, k_n is the factor of shear distribution along the normal axis and $k_n = 6/5$ for rectangular cross-section.

The configuration of a circular stepped beam considered in this study is given in Fig. 2. In order to use the exact solution of Eq. (1) given by Tufekci and Arpaci (1998), this curved beam is divided into three sub-domains with constant cross-sections. For each sub-domain, the Eq. (1) can be written by using the following boundaries

For the first sub-domain: $-\phi_A \le \phi_1 \le -\psi_1 \qquad \dfrac{d\mathbf{y}_1}{d\phi_1} = \mathbf{A}_1(\phi_1)\mathbf{y}_1(\phi_1)$

For the second sub-domain: $-\psi_1 \le \phi_2 \le -\psi_2 \qquad \dfrac{d\mathbf{y}_2}{d\phi_2} = \mathbf{A}_2(\phi_2)\mathbf{y}_2(\phi_2)$

For the third sub-domain: $\psi_2 \le \phi_3 \le \phi_B \qquad \dfrac{d\mathbf{y}_3}{d\phi_3} = \mathbf{A}_3(\phi_3)\mathbf{y}_3(\phi_3)$ (2)

According to the procedure by Tufekci and Arpaci (1998), the exact solution of Eq. (2) can be obtained as

$$\mathbf{y}_1(\phi_1) = e^{\mathbf{A}_1\phi_1}\mathbf{y}_1(\phi_{01})$$
$$\mathbf{y}_2(\phi_2) = e^{\mathbf{A}_2\phi_2}\mathbf{y}_2(\phi_{02})$$
$$\mathbf{y}_3(\phi_3) = e^{\mathbf{A}_3\phi_3}\mathbf{y}_3(\phi_{03}) \tag{3}$$

provided that the initial values vectors $\mathbf{y}_1(\phi_{01}), \mathbf{y}_2(\phi_{02}), \mathbf{y}_3(\phi_{03})$ at the reference coordinates $\phi_1 = \phi_{01}$, $\phi_2 = \phi_{02}$, $\phi_3 = \phi_{03}$ are known. The terms $e^{\mathbf{A}_1\phi_1}, e^{\mathbf{A}_2\phi_2}$ and $e^{\mathbf{A}_3\phi_3}$ can be expressed exactly. The initial values vectors must be obtained in order to specify the solution vectors $\mathbf{y}_1(\phi_{01}), \mathbf{y}_2(\phi_{02})$ and $\mathbf{y}_3(\phi_{03})$. Eighteen elements of these vectors can be found by using 18 equations obtained from the boundary conditions at the ends A, B and the kinetic and kinematic continuity conditions at points C ($\phi_1 = -\psi_1, \phi_2 = -\psi_1$) and D ($\phi_2 = \psi_2, \phi_3 = \psi_2$).

2.1 Boundary conditions

For end A in Fig. 2

$$\begin{aligned}
&\text{Hinged end:} \quad w_1(-\phi_A) = 0; \quad u_1(-\phi_A) = 0; \quad M_{b1}(-\phi_A) = 0\\
&\text{Clamped end:} \quad w_1(-\phi_A) = 0; \quad u_1(-\phi_A) = 0; \quad \Omega_{b1}(-\phi_A) = 0\\
&\text{Free end:} \quad M_{b1}(-\phi_A) = 0; \quad F_{t1}(-\phi_A) = 0; \quad F_{n1}(-\phi_A) = 0
\end{aligned} \tag{4}$$

Similar expressions are specified for the end B in Fig. 2. These conditions yield six simultaneous linear equations in terms of the initial values at the reference coordinates $\phi_1 = \phi_{01}$ and $\phi_2 = \phi_{02}$.

2.2 Kinematic and kinetic continuity conditions

At the boundaries of the sub-domains, the continuity conditions between the adjacent portions have to be expressed. The continuity and equilibrium conditions at the boundaries of the portions at point C and D require that all quantities at these boundaries of the portions must be equal to each other

$$\begin{aligned}
\mathbf{y}_1(-\psi_1) &= \mathbf{y}_2(-\psi_1) \qquad & e^{-\mathbf{A}_1\psi_1}\mathbf{y}_{01} &= e^{-\mathbf{A}_2\psi_1}\mathbf{y}_{02}\\
\mathbf{y}_2(\psi_2) &= \mathbf{y}_3(\psi_2) \qquad & e^{\mathbf{A}_2\psi_2}\mathbf{y}_{02} &= e^{\mathbf{A}_3\psi_2}\mathbf{y}_{03}
\end{aligned} \tag{5}$$

This also yields twelve simultaneous linear equations in terms of the initial values at the reference coordinates $\phi_0 = \phi_{01}, \phi_2 = \phi_{02}$ and $\phi_3 = \phi_{03}$.

Thus, the eighteen equations associated with the boundary and continuity conditions can be written in matrix form

$$\begin{bmatrix} \mathbf{X1} & \mathbf{01} & \mathbf{01} \\ e^{-\mathbf{A}_1\psi_1} & -e^{-\mathbf{A}_2\psi_1} & \mathbf{02} \\ \mathbf{02} & e^{\mathbf{A}_2\psi_2} & e^{-\mathbf{A}_3\psi_2} \\ \mathbf{01} & \mathbf{01} & \mathbf{X2} \end{bmatrix}_{18\times 18} \cdot \begin{bmatrix} \mathbf{y}_{01} \\ \mathbf{y}_{02} \\ \mathbf{y}_{03} \end{bmatrix}_{18\times 1} = [\mathbf{0}]_{18\times 1} \tag{6}$$

where $\mathbf{y}_{01} = \mathbf{y}_1(\phi_{01})$, $\mathbf{y}_{02} = \mathbf{y}_2(\phi_{02})$ and $\mathbf{y}_{03} = \mathbf{y}_3(\phi_{03})$, **X1** and **X2** are 3×6 matrices obtained from the boundary conditions at the ends A and B; **01**'s and **02**'s are 3×6 and 6×6 zero matrices respectively. The determinant of the coefficient matrix must equal to zero in order to get the non-trivial solution of these linear homogeneous equations. The natural frequencies can be determined by finding the roots of the frequency equation. It is also possible to apply this solution procedure to other cases in which some effects are neglected.

3. Numerical evaluations and comparisons

The proposed method is applied to obtain the natural frequencies of the stepped arch with various boundary conditions (clamped-clamped, hinged-hinged, free-free, hinged-clamped and clamped-free) and geometry parameters. The geometry parameters considered here are the opening angle of the arch ϕ_T, the position parameter of the step ψ_1/ϕ_T which is illustrated in Fig. 2, the opening angles ratio ψ_T/ϕ_T which is denoted by ξ, the slenderness ratio $\lambda = R/i$, where i is the radius of gyration and the step ratio h_2/h_1 which is denoted by η. It is assumed that $h_3 = h_1$, unless otherwise specified. The numerical examples are evaluated to show the effects of the variation of all these geometry parameters on the frequency coefficient. The frequency coefficient is given as $c = \omega R^2\phi_T^2(\mu_1/EI_{b1})^{1/2}$ and calculated for five different cases.

Case 1: No effect is considered (the Euler-Bernoulli beam theory in which the effects of axial extension, shear deformation and rotatory inertia are not considered).

Case 2: All effects are considered.

Case 3: Only shear deformation effect is considered.

Case 4: Only rotatory inertia effect is considered.

Case 5: Only axial extension effect is considered.

The numerical results are obtained for ϕ_T = 10°, 20°, 30°, 60°, 90°, 135°, 180°; $\eta = h_2/h_1$ = 0.4, 0.6, 0.8, 1, 1.2, 1.4, 1.6, 1.8, 2; $\xi = \psi_T/\phi_T$ = 0.2, 0.4, 0.6; ψ_1/ϕ_T = −0.4, −0.3, −0.2, −0.1, 0.0, 0.1, 0.2; $\lambda = R/i$ = 50, 100, 150.

Fig. 3 presents the non-dimensional frequencies for different opening angles, ϕ_T, with the different cases considering axial extension, transverse shear deformation and rotatory inertia effects individually. It can be seen that the axial extension is the major effect. It is not possible to model the realistic beam behavior by neglecting the axial extension effect. As it is expected, the rotatory inertia has little effect for the first mode. The frequency coefficient increases sharply for small opening angle and then decreases slowly for larger opening angles. Similar characteristics can be

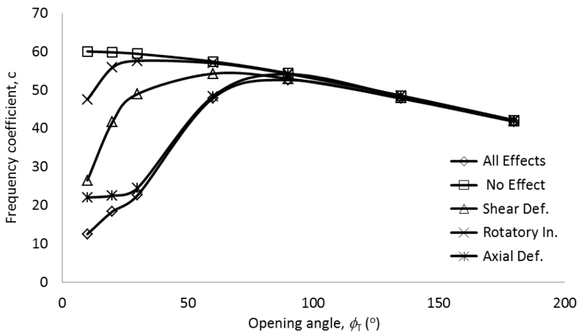

Fig. 3 The first frequency coefficient for a clamped-clamped arch with λ = 50, ψ_T/ϕ_T = 0.2, ψ_1/ϕ_T = −0.4, η = 0.8

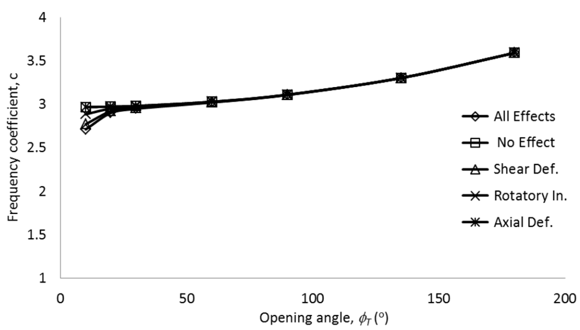

Fig. 4 The first frequency coefficient for a clamped-free arch with λ = 50, ψ_T/ϕ_T = 0.2, ψ_1/ϕ_T = −0.4, η = 0.8

seen for the other symmetric boundary conditions such as hinged-hinged and free-free. The unsymmetrical type of boundary conditions such as hinged-clamped and clamped-free are also investigated. The figures for other boundary conditions are very similar to those given in the present paper and they are not presented here for the brevity.

The mode transition phenomenon for this arch is observed around the angle of 60° in Fig. 3. The mode shape changes significantly from extensional into inextensional. As the slenderness ratio increases, the mode transition occurs in smaller angles.

The results of clamped-free boundary condition for different cases are illustrated in Fig. 4. The slenderness ratio is 50 and the subtended angle of the arch changes from 10° to 180°. The effects of the cases on the first frequency are shown in this figure. The results of the cases are considerably close to each other for all opening angles. While the axial extension effect does not change the frequency, the major effect is the shear deformation effect in this boundary condition, as it is expected. The frequency coefficient increases with increasing opening angle. This is significantly different from those of other boundary conditions. This different characteristic of frequency curve is not observed in higher modes.

Fig. 5 gives a comparison for the first frequency coefficients of all boundary conditions. The frequency coefficients increase sharply for small opening angles and then decrease slowly for clamped-clamped (C-C), hinged-clamped (H-C), hinged-hinged (H-H) and also free-free (F-F) boundary conditions. But the first frequency coefficient of a clamped-free (C-F) beam increases when the opening angle increases. This different characteristic is not observed for the higher modes.

Fig. 6 shows the first frequency coefficient of a clamped-free beam for different values of the position parameter ψ_1/ϕ_T. As it can be seen in the figure, the frequency coefficient is affected slightly by the position parameter. The frequency coefficient increases for all opening angles, as the step position parameter increases.

The Figs. 7 and 8 give the variation of frequency coefficients with the position parameter for hinged-hinged and clamped-free beams having different step ratios. As it can be seen in Fig. 7, the frequency coefficient will be minimum for $h_2/h_1 = 1.2$ and maximum for $h_2/h_1 = 0.8$ at the position parameter of step $\psi_1/\phi_T = -0.1$, where the stepped portion is at the crown of the beam. In Fig. 8, for the step ratio $h_2/h_1 = 0.8$, the first frequency of a clamped-free beam increases, as the position parameter, ψ_1/ϕ_T, increases. But, for the step ratio $h_2/h_1 = 0.8$, the frequency decreases when the step

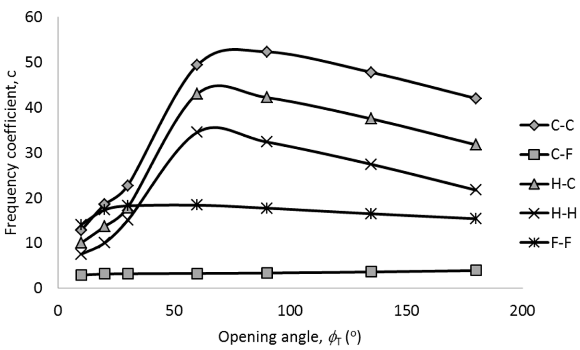

Fig. 5 The frequency coefficients of arches with different boundary conditions $\lambda = 50$, $\psi_T/\phi_T = 0.2$, $\psi_1/\phi_T = -0.2$, $\eta = 0.8$

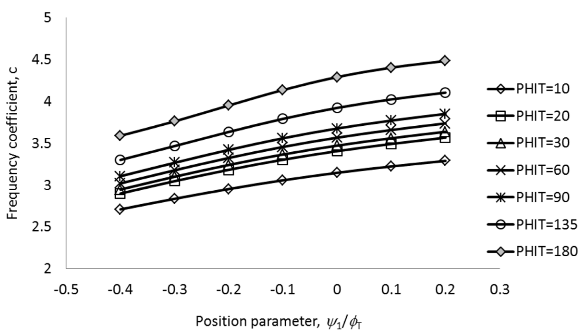

Fig. 6 The effect of step position parameter on the first frequency coefficients for a clamped-free arch with $\lambda = 50$, $\psi_T/\phi_T = 0.2$, $\eta = 0.8$

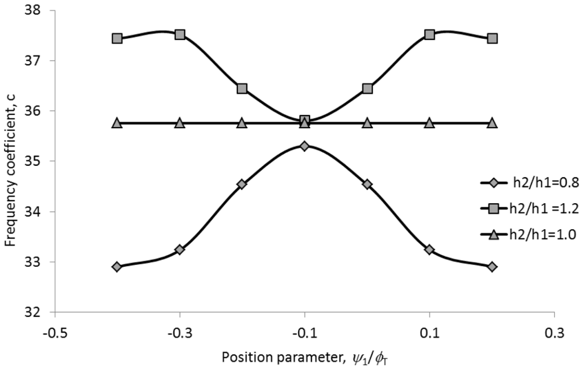

Fig. 7 The effect of step position parameter on the frequency coefficient for a hinged- hinged arch with λ = 50, ϕ_T= 60°, ψ_T/ϕ_T= 0.2

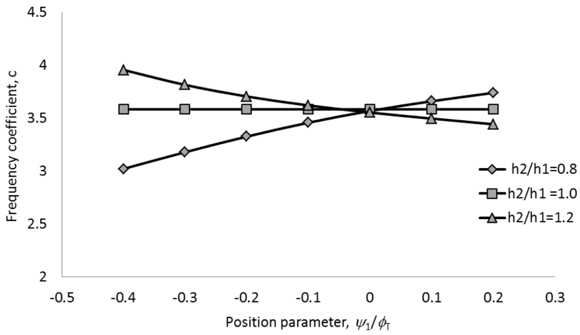

Fig. 8 The effect of step position parameter and step ratio on the first frequency coefficients for a clamped-free arch with λ = 50, ϕ_T = 60°, ψ_T/ϕ_T = 0.2

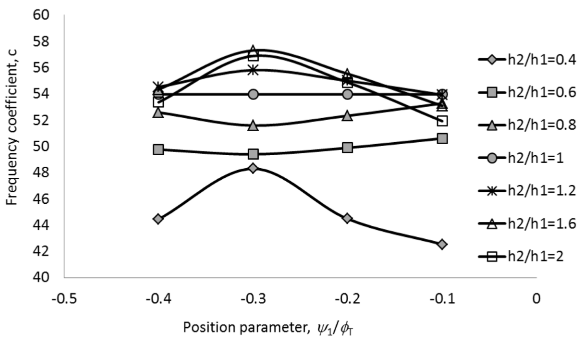

Fig. 9 The effect of position parameter on the frequency coefficients for a clamped-clamped arch with λ = 50, ψ_T/ϕ_T = 0.2 and ϕ_T = 90°

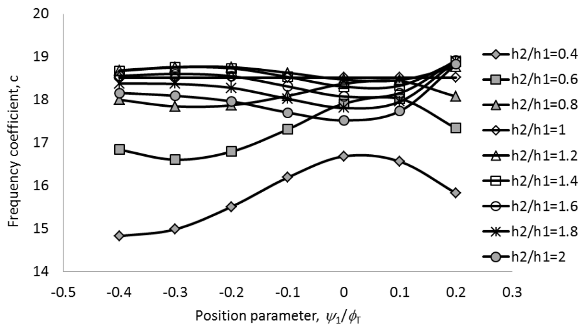

Fig. 10 The effect of position parameter on the frequency coefficients of a hinged-clamped arch with λ = 50, ψ_T/ϕ_T= 0.2 and ϕ_T = 30°

subdomain moves from the clamped end to the free end.

Fig. 9 shows the effect of position parameter on the first frequency of a clamped-clamped beam. The frequency coefficients have the maximum values around $\psi_1/\phi_T = -0.3$ for h_2/h_1 = 0.4, 1.2, 1.6 and 2.0, and the minimum values when the stepped subdomain is in the middle of the beam. The frequency coefficients have the minimum values around $\psi_1/\phi_T = -0.3$ and the maximum values around $\psi_1/\phi_T = -0.1$ for $h_2/h_1 = 0.6$ and 0.8. The similar characteristics for other symmetric boundary conditions can be observed.

The effect of the position parameter on the first frequency of a hinged-clamped beam is given in Fig. 10. The frequency curves have the maximum values between ψ_1/ϕ_T = 0 and 0.1 for the step ratio of $h_2/h_1 < 1$, and the minimum values between ψ_1/ϕ_T = 0 and 0.1, for $h_2/h_1 > 1$.

Fig. 11 presents the effect of the position parameter on the frequency coefficient of a clamped-free beam. The frequency coefficient increases for $h_2/h_1 < 1$ and decreases for $h_2/h_1 > 1$, as position parameter increases. When the stepped portion moves from the clamped end to the free end, for the step ratio $h_2/h_1 < 1$, the frequency increases, and for $h_2/h_1 > 1$, the frequency decreases.

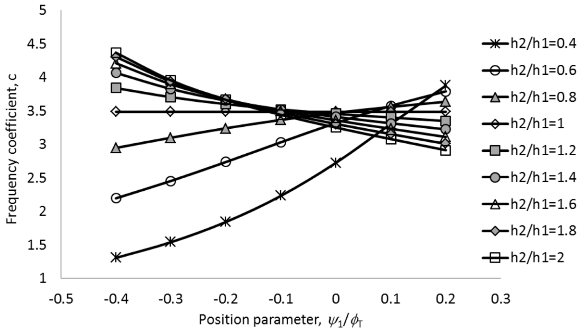

Fig. 11 The effect of position parameter on the frequency coefficients for a clamped-free arch with $\lambda = 50$, $\psi_T/\phi_T = 0.2$ and $\phi_T = 30^o$

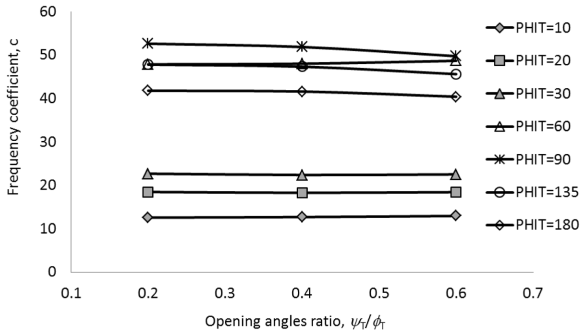

Fig. 12 The effect of step ratio on the frequency coefficients for a clamped-clamped arch with $\lambda = 50$, $\psi_1/\phi_T = -0.4$, $\eta = 0.8$

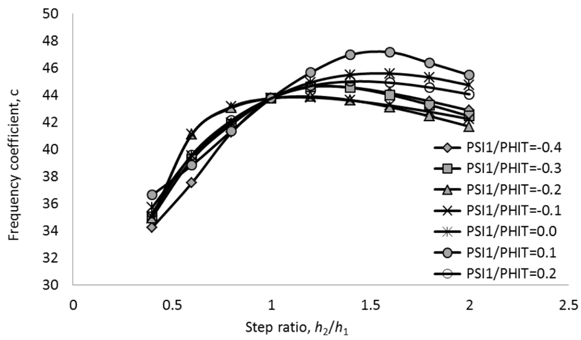

Fig. 13 The effect of step ratio on the frequency coefficients for a hinged-clamped arch with $\lambda = 50$, $\psi_T/\phi_T = 0.2$ and $\phi_T = 60^o$

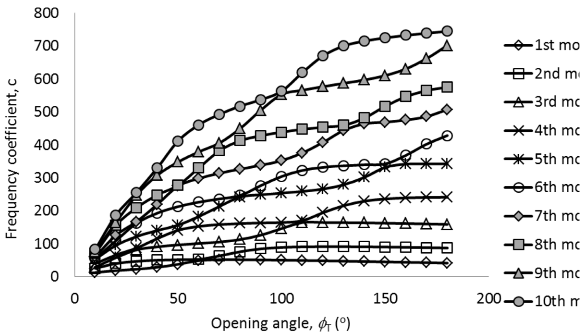

Fig. 14 The first ten frequency coefficients of a clamped-clamped arch with $\lambda = 50$, $\psi_T/\phi_T = 0.4$, $\psi_1/\phi_T = -0.3$, $\eta = 0.8$

In Fig. 12, the effects of the opening angles ratio, ψ_T/ϕ_T, on the frequency coefficients of a clamped-clamped arch are given for different opening angles. As it can be seen in the figure, the frequency coefficient is affected slightly by the position parameter. There is a continuous decrease for $\phi_T = 90^o$, 135^o, and 180^o while there is a continuous increase for $\phi_T = 10^o$, 20^o, 30^o and 60^o.

The effect of the step ratio on the first frequency for a hinged-clamped beam is presented in Fig. 13. For the step position parameter of $\psi_1/\phi_T = -0.1$ and -0.2, the frequency increases sharply until the step ratio of $h_2/h_1 = 1.0$, and then decreases slightly. For the step position parameter of $\psi_1/\phi_T = -0.4$ and -0.3, the frequency reaches the maximum value around $h_2/h_1 = 1.2$. For the step position parameter of $\psi_1/\phi_T = 0.0$, 0.1 and 0.2, the maximum of the frequency can be found around $h_2/h_1 = 1.4$. The similar diagrams are obtained for other boundary conditions. The frequency coefficients are a strong function of the position parameter for all step ratios.

The first ten frequency coefficients of a clamped-clamped arch are given in Fig. 14. The examinations are performed for the case in which all effects are taken into consideration. The other boundary conditions, step ratios and position parameters do not change the characteristic of these curves. The mode transition phenomenon occurs in the opening angles in which the curves approach each other. The mode shapes change from one configuration to another. For example, in Fig. 14, for

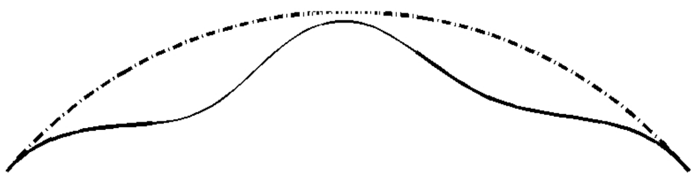

(a) The third mode shape, ϕ_T=100°, f_3=1826.09 Hz

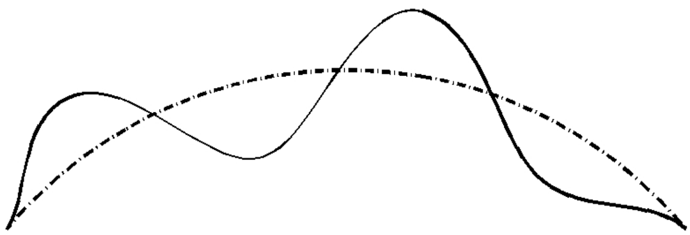

(b) The fourth mode shape, ϕ_T=100°, f_4=2052.49 Hz

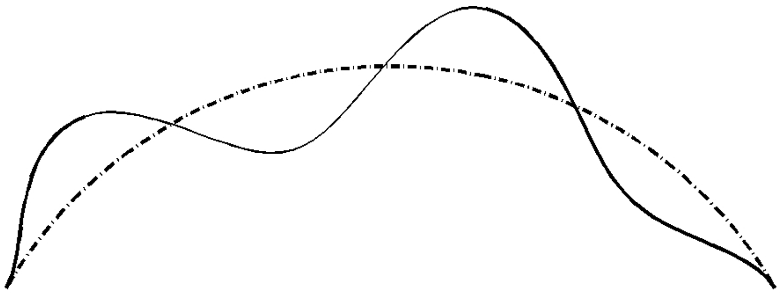

(c) The third mode shape, ϕ_T=120°, f_3=1427.01 Hz

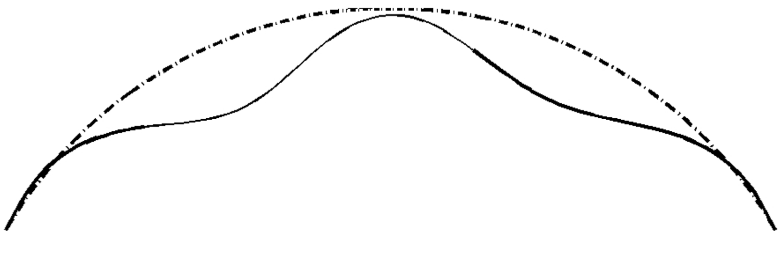

(d) The fourth mode shape, ϕ_T=120°, f_4=1686.64 Hz

Fig. 15 The third and fourth mode shapes of clamped-clamped arches, λ = 50, h_2/h_1 = 0.8, ψ_1/ϕ_T = −0.3, ψ_T/ϕ_T = 0.4

the beam with ϕ_T = 100°, the third mode shape is the same as the fourth mode shape for the beam with ϕ_T = 120°. Fig. 15 gives the third and fourth mode shapes of circular beams with opening angles of 100° and 120°. As it can be seen from the figure, the third mode shape of the beam with ϕ_T = 100° is the same as the fourth mode shape of the beam with ϕ_T = 120°.

Numerical calculations for the same problem were performed also using commercial finite

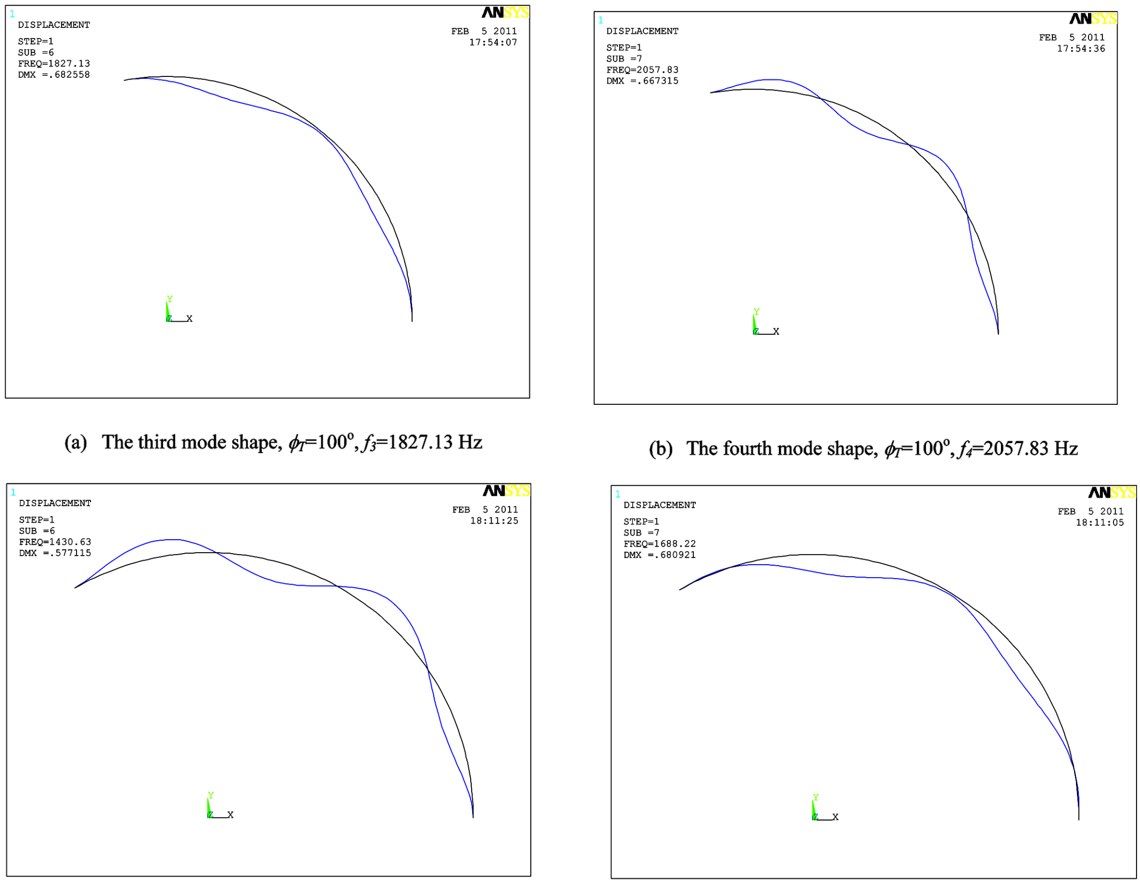

(a) The third mode shape, ϕ_T=100°, f_3=1827.13 Hz

(b) The fourth mode shape, ϕ_T=100°, f_4=2057.83 Hz

(c) The third mode shape, ϕ_T=120°, f_3=1430.63 Hz

(d) The fourth mode shape, ϕ_T=120°, f_4=1688.22 Hz

Fig. 16 The third and fourth mode shapes of clamped-clamped arches (ANSYS results), λ = 50, h_2/h_1 = 0.8, ψ_1/ϕ_T = –0.3, ψ_T/ϕ_T = 0.4

element analysis software ANSYS (version 13) and converged solutions based on the 2-node beam element Beam188 are given in Fig. 16. The frequencies are in very good agreement with the analytical results. The mode shapes are exactly same as those obtained by the analytical method. The third mode shape of the beam with ϕ_T = 100° is the same as the fourth mode shape of the beam with ϕ_T = 120°. It can be seen from the Figs. 14-16 that the mode transition is observed in the third and fourth modes around the opening angle of ϕ_T = 110°.

The comparisons of the results of different solution methods in literature and this study are given in tables. The classical approximate Ritz and Galerkin approaches have been extensively applied in a large number of investigations, both in their classical version and in the modified Rayleigh-Schmidt version. Clamped-clamped, hinged-hinged and hinged-clamped boundary conditions are examined and comparisons of the results of the Rayleigh-Ritz (R-R), finite element method (FEM) and the cells discretization method (CDM) in the references are performed.

The first non-dimensional natural frequencies for stepped arches are obtained for different parameters: Opening angle of the arch ϕ_T, the position parameter of the step ψ_1/ϕ_T, opening angles ratio ($\xi = \psi_T/\phi_T$), the slenderness ratio ($\lambda = R/i$), the step ratio ($\eta = h_2/h_1$). The discontinuity of arch is considered at the crown of the arch and the different position of stepped subdomain and the opening angles ratios have not been included in almost all of the studies in the literature. In the following tables, the slenderness ratio is taken as $\lambda = R/i = 50$ for Case 2.

In Tables 1 and 2, the first non-dimensional frequencies from the Rayleigh-Ritz, the cells discretization (CDM) and the finite element (FEM) methods (the commercial program SAP IV was used) (Auciello and De Rosa 1994) for different step ratios and opening angles are compared with those obtained in this study. In these tables, two sets of exact solutions, Case 1 (no effect) and Case 2 (all effects), are given. These two sets give close results for large opening angles, while the differences are considerable for smaller angles. As it can be seen from Tables 1 and 2, the results of Auciello and De Rosa (1994) are very close to the exact solutions of Case 1, since this reference neglects the effects of axial extension, shear deformation and rotatory inertia. All effects have to be considered in order to obtain the correct natural ferquencies for the beams with smaller opening angles. Tong *et al*. (1998) also solved the same problem and their results are given in Table 2. It can be seen that their results are in well agreement with those of this study.

Verniere De Irassar and Laura (1987) studied the natural frequencies of clamped-clamped and

Table 1 The first non-dimensional frequency ($c = \omega R^2\sqrt{\mu_1/EI_1}$) for clamped-clamped stepped arch (ψ_T/ϕ_T = 0.5, $\psi_1/\phi_T = -0.375$, $\lambda = R/i = 50$ for Case 2)

	$\eta = 0.8$				$\eta = 1.2$			
ϕ_T	Auciello and De Rosa (1994)		This Study		Auciello and De Rosa (1994)		This Study	
	R-R	CDM	Case 1	Case 2	R-R	CDM	Case 1	Case 2
5	7656.8	7216.57	7524.508	995.785	8519.54	8639.3	8563.159	927.356
10	1913.9	1802.62	1879.500	423.746	2129.23	2157.5	2138.546	409.841
20	478.06	449.142	468.255	151.225	531.73	537.08	532.404	154.026
30		198.508	206.925	82.189		237.01	234.988	84.608
40	119.1	110.798	115.472	58.568	132.297	132.01	130.914	59.592
45	93.997	87.1349	90.800	52.890	104.336	103.69	102.839	53.404
50		70.2129	73.156	49.134		83.439	82.764	49.297
60		48.1797	50.183	44.143		57.076	56.631	44.355
70		34.907	36.345	34.613		41.204	40.895	38.286
80		26.306	27.378	26.398		30.925	30.705	29.224
90	23.089	20.421	21.243	20.636	25.46	23.9	23.739	22.813
100		16.2238	16.868	16.472		18.897	18.776	18.169
110		13.1297	13.643	13.375		15.215	15.122	14.710
120		10.7872	11.202	11.014		12.433	12.361	12.073
130		8.9744	9.313	9.179		10.285	10.228	10.023
140		7.5456	7.825	7.726		8.5962	8.551	8.401
150		6.40186	6.634	6.560		7.2483	7.212	7.101
160		5.4741	5.668	5.612		6.1582	6.129	6.045
170		4.71299	4.875	4.832		5.2667	5.242	5.179
180		4.0823	4.219	4.186		4.5305	4.510	4.461

hinged-hinged stepped arches by using Rayleigh-Ritz method. The effects of axial extension, shear deformation and rotatory inertia are neglected in the calculations. Table 3 gives the second non-dimensional frequencies of both clamped-clamped and hinged-hinged stepped curved beams for several opening angles and step ratios. The results of Verniere De Irassar and Laura (1987) and this study are compared in Table 3. The results are close to those obtained by neglecting all effects (Case 1).

Laura *et al*. (1988) considered the free vibrations of stepped beams with clamped-clamped and hinged-hinged ends by using the optimized Ritz procedure. The calculations were performed for several opening angles and step ratios by neglecting the effects of axial extension, shear deformation and rotatory inertia. The FEM results were also obtained by using finite element analysis program SAP IV. The finite element analyses were performed for hinged-hinged arch with opening angle of ϕ_T = 20º and several step ratios. The results are given in Table 4. As it can be seen, the results are in well agreement with those of this study for Case 1. The FEM results are much closer to the exact results of Case 1 than those of the Ritz method. The results of Case 2 are obtained for beams with λ = 50.

Rossi and Laura (1995) studied the dynamic stiffening of simply supported and clamped arches. The effects of axial extension, shear deformation and rotatory inertia are included in the analyses.

Table 2 The first non-dimensional frequency ($c = \omega R^2\sqrt{\mu_1/EI_1}$) for clamped-clamped stepped arch (η = 0.8, ψ_T/ϕ_T = 0.5, ψ_1/ϕ_T = –0.35, $\lambda = R/i$ = 50 for Case 2)

ϕ_T	Auciello and De Rosa (1994)			Tong *et al.* (1998)	This Study	
	R-R	FEM	CDM		Case 1	Case 2
5	7836.7		7368.8		7451.01	1002.88
10	1958.9		1840.9	1844.84	1861.16	426.98
20	489.3	456.31	458.68	459.662	463.701	152.415
30			202.72	203.157	204.923	82.818
40	121.87	113.195	113.15	113.392	114.363	58.991
45	96.166		88.987	89.175	89.932	53.263
50			71.705	71.856	72.4604	49.477
60			49.2	49.306	49.7121	44.374
70			35.647	35.722	36.009	34.354
80			26.86	26.918	27.1291	26.184
90	23.599		20.851	20.895	21.054	20.468
100			16.564		16.721	16.338
110			13.403		13.527	13.268
120			11.009		11.1097	10.928
130			9.1565		9.2389	9.1086
140			7.6961		7.7646	7.6692
150			6.5269		6.5845	6.5135
160			5.5784		5.6275	5.5738
170			4.8001		4.8423	4.8013
180			4.155		4.1919	4.1601

Table 3 The second non-dimensional frequency ($c = \omega R^2 \phi_T^2 \sqrt{\mu_1/EI_1}$) of Verniere De Irassar and Laura (1987), RR: Rayleigh-Ritz method (ψ_T/ϕ_T = 0.4, ψ_1/ϕ_T = –0.2, and λ = 50 for Case 2)

ϕ_T	η	Clamped-clamped			Hinged-hinged		
		RR	This Study		RR	This Study	
			Case 1	Case 2		Case 1	Case 2
5	1	114.436	110.979	13.54926	85.282	84.2868	10.77567
	1.2	116.849	115.413	12.53338	88.423	88.5597	9.724393
	1.4	121.304	120.487	11.03094	93.322	93.4875	8.580487
10	1	114.419	110.939	25.3753	85.26	84.2453	23.28559
	1.2	116.829	115.369	24.69023	88.399	88.5146	23.45347
	1.4	121.28	120.438	23.51548	93.294	93.4384	22.85385
20	1	114.36	110.777	40.93305	85.175	84.0795	31.90491
	1.2	116.748	115.19	41.14845	88.303	88.3343	32.6872
	1.4	121.184	120.242	40.6088	93.184	93.2424	32.70176
30	1	114.238	110.507	48.71901	85.033	83.8041	34.9088
	1.2	116.613	114.894	49.67656	88.142	88.0349	35.98568
	1.4	121.025	119.917	49.62477	93.001	92.9166	36.2154
40	1	114.079	110.131	52.50476	84.835	83.4203	35.91803
	1.2	116.425	114.481	53.93591	87.917	87.6176	37.11917
	1.4	120.802	119.463	54.1942	92.744	92.4627	37.44048
45	1	113.983	109.904	53.56997	84.714	83.1883	36.06533
	1.2	116.311	114.231	55.15398	87.78	87.3654	37.29084
	1.4	120.666	119.189	55.51266	92.596	92.1883	37.63073
60	1	113.628	109.068	54.96573	84.267	82.3351	48.46284
	1.2	115.889	113.312	56.78264	87.432	86.4377	47.51779
	1.4	120.166	118.18	57.29274	92.013	91.179	46.68427

Finite element algorithmic procedure was used. The slenderness ratio was described as $i/(R\phi_T)$ and taken as 0.05. The results of the first six frequency coefficients are compared with those of this study in Table 5. The authors think that the third frequency coefficient, in the reference paper, of clamped-clamped arch with opening angle of 180° and the step ratio of 0.8 was given as 43.843 by mistake instead of 73.843, which is given as bold characters in Table 5. The results of Rossi and Laura (1995) are extremely close to the exact results of this study. As it can be seen, some frequencies of successive modes are very close to each other and the mode transition phenomenon can be observed around this opening angle. For example, the third and fourth mode frequencies of the clamped-clamped arch with opening angle of 60° and the step ratio of 0.6 are very close to each other and the mode shapes, around this opening angle, are changes from one configuration to another. Similar case can be observed for the first and second frequencies of hinged-hinged arch with opening angle of 90° and the step ratio of 0.8.

Tables 6-8 give the first frequency coefficient for several opening angles ratios of ψ_T/ϕ_T = 1/4, 1/3 and 1/2, and step position parametes ψ_1/ϕ_T = –1/8, –1/6, and –1/4. For the brevity, the first six

Table 4 The first non-dimensional frequency ($c = \omega R^2 \phi_T^2 \sqrt{\mu_1/EI_1}$) of Laura *et al*. (1988), ($\psi_T/\phi_T = 0.5$, $\psi_1/\phi_T = -0.25$; and $\lambda = 50$ for Case 2)

ϕ_T	η	Clamped-clamped			Hinged-hinged			
		Ritz	This Study		Ritz	FEM	This Study	
			Case 1	Case 2			Case 1	Case 2
5	0.8	58.31	55.1665	7.7465				
	1	60.91	61.6529	7.3193	38.26		39.4594	5.86404
	1.2	64.88	66.3636	6.9685	41.45		42.471	6.00704
	1.4	70.1	69.283	6.6648	45.34		44.0381	5.97385
10	0.8	58.3	55.1199	13.191				
	1	60.9	61.5933	12.737	38.24		39.4024	8.16437
	1.2	64.86	66.2926	12.384	41.43		42.4052	8.824
	1.4	70.67	69.2025	12.059	45.31		43.9655	9.16221
20	0.8	58.25	54.9344	18.838				
	1	60.84	61.356	18.706	38.15	39.02	39.1756	10.7217
	1.2	64.79	66.0099	18.748	41.33	41.98	42.1435	11.666
	1.4	69.98	68.8826	18.792	45.21	43.49	43.6772	12.3175
30	0.8							
	1				38		38.8021	15.5057
	1.2				41.16		41.7133	16.1103
	1.4				45.02		43.2038	16.5612
40	0.8	58.05	54.2048	29.181				
	1	60.59	60.4246	28.929	37.08	38.26	38.2882	23.7372
	1.2	64.48	64.9029	28.964	40.94	41.08	41.1228	23.8333
	1.4	69.6	67.6325	29.11	44.77	42.51	42.5556	23.8907
45	0.8	57.97	53.9511	33.366				
	1	60.5	60.1014	32.928	37.67		37.9813	29.0307
	1.2	64.36	64.5197	32.792	40.81		40.7708	28.8678
	1.4	69.46	67.2007	32.801	44.62		42.1699	28.7144
90	0.8	56.97	50.571	49.275				
	1	59.24	55.8252	53.967	35.9		33.9605	33.4635
	1.2	62.82	59.4907	57.075	38.83		36.2113	35.5832
	1.4	67.58	61.5811	58.698	42.43		37.2249	36.5014

frequencies are not compared in the tables. The results of Rossi and Laura (1995) are in well agreement with the results of this study.

Viola *et al.* (2007) investigated the in-plane free vibration problem of multi-stepped and multi-damaged arches with different boundary conditions. The analyses were performed by using both analytical method based on the Euler characteristic exponent procedure and the numerical method, generalized differential quadrature element (GDQE) technique. The first ten frequencies of arches

Table 5 The non-dimensional frequencies ($c = \omega R^2 \phi_T^2 \sqrt{\mu_1/EI_1}$) for different step ratio (RL: Rossi and Laura 1995) ($\psi_T/\phi_T = 0.2$, $\psi_1/\phi_T = -0.1$, and $i/(R\phi_T) = 0.05$)

ϕ_T (°)	Mode No.	Clamped-clamped				Hinged-hinged			
		$\eta = 0.6$		$\eta = 0.8$		$\eta = 0.6$		$\eta = 0.8$	
		RL	Case 2	RL	Case 2	RL	Case 2	RL	Case 2
20	1	18.678	18.63896	19.315	19.2898	9.282	9.241534	10.535	10.51651
	2	41.763	41.68504	43.523	43.42459	31.213	31.17326	32.749	32.33543
	3	68.372	68.30448	65.685	65.65409	61.298	61.08867	63.424	63.19179
	4	70.437	70.13246	72.755	72.41738	68.368	68.30207	65.660	66.01205
	5	99.760	99.01473	106.32	105.3800	93.077	92.46856	99.353	98.57928
	6	116.13	115.8252	121.84	121.4582	116.11	115.817	121.79	121.4384
40	1	21.336	21.2047	21.792	21.7093	14.36	14.24645	15.123	15.06232
	2	41.056	40.92896	42.646	42.46763	30.518	30.43807	31.953	31.84299
	3	68.990	68.95757	66.532	66.60929	60.911	60.60486	63.077	62.73704
	4	70.173	69.76209	72.226	72.08725	68.982	68.95305	66.456	66.52973
	5	99.810	99.04241	106.27	105.2528	93.082	92.45327	99.256	98.37627
	6	116.20	116.2006	121.62	121.5921	116.15	116.1637	121.73	121.6863
60	1	25.101	24.83377	25.330	25.15404	20.125	20.43896	20.565	19.91771
	2	39.964	39.77252	41.330	41.05197	29.423	29.28799	30.715	30.52681
	3	69.757	69.1901	67.783	67.9962	60.287	59.83821	62.526	62.02554
	4	69.914	69.91001	72.226	71.29299	69.909	69.90904	67.671	67.88755
	5	99.914	99.1211	106.27	105.0703	93.124	92.4813	99.116	98.07729
	6	116.20	116.7879	121.62	122.2525	116.20	116.6878	121.62	122.0271
90	1	31.79	31.2273	31.635	31.23432	27.193	26.97354	28.246	27.94254
	2	37.817	37.52512	38.832	38.41455	29.060	28.63469	29.118	28.8126
	3	68.943	68.11426	70.067	70.4469	58.986	58.30738	61.439	60.65877
	4	71.598	71.55319	71.656	70.6869	71.595	71.53171	69.980	70.38489
	5	100.24	99.44341	106.28	104.7968	93.379	92.79715	98.916	97.59926
	6	116.60	117.9454	121.95	123.1286	116.31	117.626	121.35	122.4751
120	1	35.312	34.94199	36.014	35.49954	24.478	24.19527	25.305	24.92147
	2	38.767	37.74511	38.149	37.3749	37.783	36.9338	37.348	36.67865
	3	68.149	67.14357	71.279	70.00516	57.522	56.74935	60.438	59.45451
	4	73.255	72.97766	72.421	72.80879	73.155	72.76459	72.411	72.80868
	5	100.89	100.2036	106.49	104.7345	94.121	93.80656	98.929	97.43129
	6	116.99	119.2224	122.04	123.9272	116.52	118.4048	120.95	122.4627
150	1	32.664	32.24842	33.104	32.53913	21.475	21.16366	22.111	21.69371
	2	45.055	43.32378	43.874	42.52436	45.054	43.30029	43.870	42.50367
	3	67.967	66.99707	71.710	70.00628	57.056	56.63866	60.798	59.86512
	4	74.508	73.75364	74.453	74.57403	74.058	73.03464	74.404	74.40135
	5	102.03	101.5928	107.05	105.1732	95.676	95.85077	99.505	98.11029
	6	117.49	120.3647	122.16	124.3562	116.52	118.6321	120.39	121.294
180	1	30.026	29.59329	30.244	29.66875	18.323	18.01936	18.804	18.39869
	2	49.331	46.73283	47.720	45.65463	47.344	44.82968	46.303	44.19681
	3	69.509	68.70979	73.843	72.23303	61.077	60.85611	64.876	63.95779
	4	75.096	73.66324	75.844	75.36939	73.986	72.17245	75.438	74.58999
	5	103.77	103.6494	108.18	106.3506	98.205	98.913	101.03	100.0607
	6	118.13	121.1933	122.34	124.2889	116.59	118.1492	119.68	120.2682

Table 6 The first non-dimensional frequency ($c = \omega R^2 \phi_T^2 \sqrt{\mu_1/EI_1}$) for stepped arch ($\psi_T/\phi_T$ = 0.25, ψ_1/ϕ_T = – 0.125, $i/(R\phi_T)$ = 0.05), RL: Rossi and Laura (1995)

	Clamped-clamped				Hinged-hinged			
	η = 0.6		η = 0.8		η = 0.6		η = 0.8	
ϕ_T (°)	RL	Case 2	RL	Case 2	RL	Case 2	RL	Case 2
20	18.938	18.89324	19.353	19.323	9.1326	9.087014	10.427	10.40495
40	21.632	21.48744	21.856	21.76279	14.338	14.21247	15.082	15.013
60	25.457	25.1643	25.432	25.23637	20.206	19.97951	20.582	20.4408
90	32.276	31.66855	31.808	31.37221	26.276	26.09361	28.003	27.71101
120	34.699	34.38216	35.894	35.39468	23.693	23.46151	25.103	24.73787
150	32.205	31.84912	33.028	32.48193	20.816	20.56212	21.945	21.54983
180	29.713	29.33669	30.208	29.65168	17.78	17.53348	18.672	18.28699

Table 7 First non-dimensional frequency ($c = \omega R^2 \phi_T^2 \sqrt{\mu_1/EI_1}$) for stepped arch ($\xi$ = 1/3 $i/(R\phi_T)$ = 0.05), RL: Rossi and Laura (1995)

	Clamped-clamped				Hinged-hinged			
	η = 0.6		η = 0.8		η = 0.6		η = 0.8	
ϕ_T	RL	Case 2	RL	Case 2	RL	Case 2	RL	Case 2
20	19.467	19.42227	19.471	19.44183	8.9823	8.928887	10.285	10.26013
40	22.188	22.03443	21.998	21.90131	14.357	14.21507	15.034	14.95669
60	26.063	25.75236	25.608	25.40497	20.361	20.11288	20.611	20.4571
90	33.004	32.36908	32.05	31.60249	24.462	24.34808	27.4	27.14862
120	33.699	33.47839	35.561	35.12205	22.1	21.95332	24.586	24.26521
150	31.455	31.1932	32.787	32.29554	19.444	19.28401	21.509	21.15718
180	29.209	28.91519	30.055	29.54269	16.623	16.47071	18.309	17.96479

Table 8 First non-dimensional frequency ($c = \omega R^2 \phi_T^2 \sqrt{\mu_1/EI_1}$) for stepped arch ($\xi$ = 0.5 $i/(R\phi_T)$ = 0.05), RL: Rossi and Laura (1995)

	Clamped-clamped				Hinged-hinged			
	η = 0.6		η = 0.8		η = 0.6		η = 0.8	
ϕ_T	RL	Case 2	RL	Case 2	RL	Case 2	RL	Case 2
20	20.1	20.19345	19.773	19.72876	8.8576	8.793438	10.106	10.07702
40	22.708	22.74091	22.268	22.17216	14.436	14.27071	14.981	14.88815
60	26.418	26.38005	25.831	25.65795	20.6	20.31963	20.651	20.4761
90	32.892	32.83958	32.157	31.82394	21.259	21.21294	25.918	25.71976
120	33.76	33.28304	35.088	34.71309	19.186	19.1322	23.254	23.002
150	31.728	31.2076	32.464	32.01369	16.853	16.80294	20.332	20.05912
180	29.703	29.15443	29.88	29.38889	14.379	14.34284	17.291	17.02894

Table 9 The results of Viola *et al.* (2007) and this study for the first ten frequencies (Hz) of two-stepped arches with different boundary conditions

Mode No.	Clamped-Clamped			Hinged-Hinged			Clamped-Free		
	Viola *et al.* (2007)		This Study	Viola *et al.* (2007)		This Study	Viola *et al.* (2007)		This Study
	Analytical	GDQE		Analytical	GDQE		Analytical	GDQE	
1	49.535	49.535	49.5345	27.564	27.564	27.5638	20.433	20.433	20.43337
2	99.224	99.224	99.2244	74.838	74.838	74.8381	67.978	67.978	67.9778
3	178.742	178.742	178.7424	140.321	140.321	140.3207	195.761	195.761	195.7612
4	261.989	261.989	261.9886	215.215	215.215	215.2151	372.498	372.498	372.498
5	366.855	366.855	366.8553	313.167	313.167	313.1669	643.913	643.913	643.9125
6	485.004	485.004	485.0036	432.367	432.367	432.3673	928.625	928.625	928.6255
7	646.009	646.009	646.0085	576.539	576.539	576.5389	1312.164	1312.164	1312.164
8	732.315	732.321	732.3207	698.877	698.877	698.8793	1478.623	1478.623	1478.623
9	865.512	865.512	865.5124	823.817	823.817	823.8152	1740.342	1740.342	1740.342
10	969.683	969.694	969.694	882.598	882.603	882.6028	2262.455	2262.455	2262.455

with clamped-clamped, hinged-hinged and clamped-free ends are given in Table 9 with the results of this study. The dimensions of clamped-clamped and hinged-hinged arches are given as: The radius of arch R = 1 m, the width b = 0.045 m, the thicknesses h_1 = 0.02 m, h_2 = 0.015 m, h_3 = 0.02 m, the opening angle ϕ_T = 120°, the opening angles ratio ψ_T/ϕ_T = –0.25, the step position parameter ψ_1/ϕ_T = 0.5. The dimensions of clamped-free arch are given as: The radius of arch R = 1 m, the width b = 0.045 m, the thicknesses h_1 = 0.03 m, h_2 = 0.025 m, h_3 = 0.015 m, the opening angle ϕ_T = 70°, the opening angles of the subdomains ϕ_1 = 20°, ϕ_2 = 20°, ϕ_3 = 30°. The results of Viola *et al.* (2007) and this study are in exteremely good agreement.

4. Conclusions

In this paper, an exact analytical solution for free in-plane vibrations of two-stepped arches is presented. The solution is obtained by using the initial values method. The exact solution developed for a uniform arch is adapted to the stepped arches. The stepped arch is divided into a number of arches with constant cross-sections. The exact solution of free vibrations of the stepped arches can be obtained in terms of the initial parameters; deformation, rotation, bending moment, normal force and shear force at one coordinate of the arch. The effects of axial extension, shear deformation and rotatory inertia are included in the analysis. The solutions are obtained also by considering each effect individually. No numerical difficulty was found in the proposed solution.

Detailed numerical results have been presented showing variations of non-dimensional frequency parameter with clamped-clamped, hinged-hinged, free-free, hinged-clamped, and clamped-free boundary conditions and with five geometric parameters for stepped arches; opening angle ϕ_T, slenderness ratio $\lambda = R/i$, step ratio $h = h_2/h_1$, position parameter ψ_1/ϕ_T and the opening angles ratio ψ_T/ϕ_T.

The numerical data reveal that increasing the value of step ratio results in smaller frequency coefficients for the first six modes. As slenderness ratio, λ, increases from 50 to 200, the frequency coefficients also increase due to the fact that the frequency coefficient contains λ.

The frequency coefficient increases sharply until some opening angle, then decreases slowly when the opening angle increases. This characteristic is almost the same for all boundary conditions except for the clamped-free arch. The significantly different characteristic is observed in the first mode; the frequency coefficient increases, as the opening angle increases, which is not observed in higher modes.

The effect of axial extension is dominant for clamped-clamped, hinged-hinged, and hinged-clamped arches while the rotatory inertia has little effect for the first mode. The shear deformation effect is the dominant for a clamped-free arch and rotatory inertia is dominant for a free-free arch.

The step position parameter affects the frequency coefficients slightly. For the symmetric boundary conditions and all opening angles, the frequency coefficient has a maximum value at the crown of the arch for $h_2/h_1 < 1$, and a minimum value for $h_2/h_1 > 1$. For a clamped-free arch, when the position parameter increases, the frequency coefficient increases slightly for step ratio $h_2/h_1 > 1$, and decreases slightly for $h_2/h_1 < 1$.

For a clamped-clamped arch with a known opening angle and opening angles ratio, the frequency coefficient has a maximum value around $\psi_1/\phi_T = -0.3$, and a minimum value when the stepped subdomain is in the middle of the beam for $h_2/h_1 = 0.4$, 1.2, 1.6 and 2.0. The frequency coefficient has the minimum value around $\psi_1/\phi_T = -0.3$ and the maximum value around $\psi_1/\phi_T = -0.1$ for $h_2/h_1 = 0.6$ and 0.8. The similar characteristics can be observed for other symmetric boundary conditions.

The frequency coefficient of a clamped-clamped arch with a given opening angle is affected slightly by the opening angles ratio, ψ_T/ϕ_T. The frequency coefficient decreases slightly for $\phi_T = 90^o$, 135^o and 180^o, and increases for $\phi_T = 10^o$, 20^o, 30^o and 60^o.

For a hinged-clamped arch, the frequency coefficients have the maximum value between $\psi_1/\phi_T =$ 0 and 0.1 for the step ratio of $h_2/h_1 < 1$, and the minimum value between $\psi_1/\phi_T = 0$ and 0.1, for $h_2/h_1 > 1$.

For a hinged-clamped arch with the step position parameter of $\psi_1/\phi_T = -0.1$ and -0.2, the frequency coefficient increases sharply until the step ratio of $h_2/h_1 = 1.0$, and then decreases slightly. For the step position parameter of $\psi_1/\phi_T = -0.4$ and -0.3, the frequency coefficient reaches the maximum value around $h_2/h_1 = 1.2$. For the step position parameter of $\psi_1/\phi_T = 0.0$, 0.1 and 0.2, the maximum of the frequency can be found around $h_2/h_1 = 1.4$. The frequency coefficients are a strong function of the position parameter for all step ratios.

For a clamped-free beam, the frequency coefficient increases for $h_2/h_1 < 1$ and decreases for $h_2/h_1 > 1$, as position parameter increases. When the stepped portion moves from the clamped end to the free end, for the step ratio $h_2/h_1 < 1$, the frequency increases, and for $h_2/h_1 > 1$ the frequency decreases.

When the first few frequency coefficients of an arch are considered, some of the successive frequency coefficients get closer to each other for some opening angles. The mode transition phenomenon occurs in the opening angles in which the curves approach each other. The mode shapes change from one configuration to another form. For example, for a clamped-clamped arch with $\lambda = 50$, $\psi_T/\phi_T = 0.4$, $\psi_1/\phi_T = -0.3$, $h_2/h_1 = 0.8$ and $\phi_T = 100^o$, the third mode shape is the same as the fourth mode shape for the beam with $\phi_T = 120^o$. When the third and fourth mode shapes of circular beams with opening angles of 100^o and 120^o are obtained analytically and/or numerically (Figs. 15 and 16), it can be seen that the third mode shape of the beam with $\phi_T = 100^o$ is the same as the fourth mode shape of the beam with $\phi_T = 120^o$.

As a result of this study, it is possible to achieve dynamic stiffening of a circular arch executing in-plane vibrations by introducing appropriate discontinuities in the cross-section. The dynamic stiffening effect is measured by means of the "dynamic stiffening efficiency parameter" which can be defined as the ratio of the frequencies of the uniform arch and stepped arch.

The results presented in the paper fill an apparent void in the vibration literature by providing the first known theoretical results for circular arches with a certain practical type of variable cross-section. Because of the high accuracy of the presented results, they can be used to compare with data obtained using modern experimental and alternative analytical methods. For other types of arches, one can directly apply the present formulation to find accurate results. Furthermore, with a simple modification, the solution given in the paper can be straightforwardly applied to analyse the free vibrations of arch with continuously varying cross-section and curvature.

References

Auciello, N.M. and De Rosa, M.A. (1994), "Free vibrations of circular arches: A review", *J. Sound Vib.*, **176**(4), 433-458.

Balasubramanian, T.S. and Prathap, G. (1989), "A field consistent higher-order curved beam element for static and dynamic analysis of stepped arches", *Comput. Struct.,* **33**, 281-288.

Chidamparam, P. and Leissa, A.W. (1993), "Vibrations of a planar curved beams, rings and arches", *Appl. Mech. Rev.*, **46**, 467-483.

Dong, G.H., Hao, S.H., Zhao, Y.P., Zong, Z. and Gui, F.K. (2010a), "Numerical analysis of the flotation ring of a gravity-type fish cage", *J. Offshore Mech. Arct.*, **132**(3), 031304.

Dong, G.H., Hao, S.H., Zhao, Y.P., Zong, Z. and Gui, F.K. (2010b), "Elastic responses of a flotation ring in water waves", *J. Fluid Struct.*, **26**(1), 176-192.

Gutierrez, R.H., Laura, P.A.A., Rossi, R.E., Berteo, R. and Villaggi, A. (1989), "In-plane vibrations of non-circular arches of non-uniform cross-section", *J. Sound Vib.*, **129**, 181-200.

Hu, Y.J., Yang, Y.J. and Kitipornchai, S. (2010), "Pull-in analysis of electrostatically actuated curved micro-beams with large deformation", *Smart Mater Struct*, **19**, 065030.

Jang, K.S., Kang, T.W., Lee, K.S., Kim, C. and Kim, T.W. (2010), "The effect of change in width on stress distribution along the curved segments of stents", *J. Mech. Sci. Technol*., **24**(6), 1265-1271.

Karami, G. and Malekzadeh, P. (2004), "In-plane free vibration analysis of circular arches with varying cross-sections using differential quadrature method", *J. Sound Vib.*, **274**, 777-799.

Karami, M.A., Yardimoglu, B. and Inman, D.J. (2010), "Coupled out of plane vibrations of spiral beams for micro-scale applications", *J. Sound Vib.*, **329**(26), 5584-5599.

Laura, P.A.A. and Maurizi, M.J. (1987), "Recent research on vibrations of arch-type structures", *Shock Vib Dig*, **19**, 6-9.

Laura, P.A.A., Verniere De Irassar, P.L., Carnicer, R. and Berteo, R. (1988), "A note on vibrations of a circumferential arch with thickness varying in a discontinuous fashion", *J. Sound Vib.*, **120**, 95-105.

Lin, H.Y. (2008), "On the natural frequencies and mode shapes of a multi-span and multi-step beam carrying a number of concentrated elements", *Struct. Eng. Mech.*, **29**(5), 531-550.

Lin, H.Y. (2010), "An exact solution for free vibrations of a non-uniform beam carrying multiple elastic-supported rigid bars", *Struct. Eng. Mech*., **34**(4), 399-416.

Liu, G.R. and Wu, T.Y. (2001), "In-plane vibration analyses of circular arches by the generalized differential quadrature rule", *Int. J. Mech. Sci.*, **43**, 2597-2611.

Lu, P., Zhao, R. and Zhang, J. (2010), "Experimental and finite element studies of special-shape arch bridge for self-balance", *Struct. Eng. Mech.*, **35**(1), 37-52.

Markus, S. and Nanasi, T. (1981), "Vibration of curved beams", *Shock Vib. Dig.*, **13**, 3-14.

Ouakad, H.M. and Younis, M.I. (2011), "Natural frequencies and mode shapes of initially curved carbon nanotube resonators under electric excitation", *J. Sound Vib.*, **330**(13), 3182-3195.

Ren, W.X., Su, C.C. and Yan, W.J. (2010), "Dynamic modeling and analysis of arch bridges using beam-arch segment assembly", *CMES-Comp. Model Eng.,* **70**(1), 67-92.
Rossi, R.E., Laura, P.A.A. and Verniere De Irassar, P.L. (1989), "In-plane vibrations of cantilevered non-circular arcs of non-uniform cross-section with a tip mass", *J. Sound Vib.*, **129**, 201-213.
Rossi, R.E. and Laura, P.A.A. (1995), "Numerical experiments on dynamic stiffening of a circular arch executing in-plane vibrations", *J. Sound Vib.*, **187**, 897-909.
Tarnopolskaya, T., De Hoog, F.R., Fletcher, N.H. and Thwaites, S. (1996), "Asymptotic analysis of the free in-plane vibrations of beams with arbitrarily varying curvature and cross-section", *J. Sound Vib.*, **196**, 659-680.
Tarnopolskaya, T., De Hoog, F.R. and Fletcher, N.H. (1999), "Low-frequency mode transition in the free in-plane vibration of curved beams", *J. Sound Vib.*, **228**, 69-90.
Tong, X., Mrad, N. and Tabarrok, B. (1998), "In-plane vibration of circular arches with variable cross-sections", *J. Sound Vib.*, **212**, 121-140.
Tufekci, E. and Arpaci, A. (1998), "Exact solution of in-plane vibrations of circular arches with account taken of axial extension, transverse shear and rotatory inertia effects", *J. Sound Vib.,* **209**, 845-856.
Tufekci, E. (2001), "Exact solution of free in-plane vibration of shallow circular arches", *Int. J. Struct. Stab. D.*, **1**, 409-428.
Tufekci, E. and Ozdemirci, O. (2006), "Exact solution of free in-plane vibration of a stepped circular arch", *J. Sound Vib.*, **295**, 725-738.
Tunay, I., Yoon, S.Y., Woerner, K. and Viswanathan, R. (2009), "Vibration analysis and control of magnet positioner using curved beam models", *IEEE T. Contr. Syst. T.*, **17**(6), 1415-1423.
Verniere De Irassar, P.L. and Laura, P.A.A. (1987), "A note on the analysis of the first symmetric mode of vibration of circular arches of non-uniform cross-section", *J. Sound Vib.*, **116**, 580-584.
Viola, E., Dilena, M. and Tornabene, F. (2007), Analytical and numerical results for vibration analysis of multi-stepped and multi-damaged circular arches", *J. Sound Vib.*, **299**(1-2), 143-163.
Xia, W. and Wang, L. (2010), "Vibration characteristics of fluid-conveying carbon nanotubes with curved longitudinal shape", *Comp. Mater. Sci.*, **49**, 99-103.
Younis, M.I., Ouakad, H.M., Alsaleem, F.M., Miles, R. and Cui, W. (2010), "Nonlinear dynamics of MEMS arches under harmonic electrostatic actuation", *J. Microelectromech. S.*, **19**(3), 647-656.
Zhou, Y., Dong, Y. and Li, S. (2010), "Analysis of a curved beam MEMS piezoelectric vibration energy harvester", *Adv. Mat. Res.*, **139-141**, 1578-1581.